Elastic misfit stress relaxation in Ino.25Gao.vsAs layers grown under tension on InP(0 0 1)

D. Jacob, Y Androussi, T Benabbas, P François, D Ferré, A Lefebvre, Michel Gendry, Y Robach

ELSEVIER

Journal of Crystal Growth 179 (1997) 331–338

JOURNAL OF CRYSTAL GROWTH

Elastic misfit stress relaxation in $In_{0.25}Ga_{0.75}As$ layers grown under tension on InP(0 0 1)

D. Jacob[a], Y. Androussi[a], T. Benabbas[a], P. François[a], D. Ferré[a], A. Lefebvre[a,*], M. Gendry[b], Y. Robach[b]

[a] *Laboratoire de Structure et Propriétés de l'Etat Solide, URA CNRS 234, Université des Sciences et Technologies de Lille, Batiment C6, F-59655 Villeneuve d'Ascq Cedex, France*

[b] *Laboratoire d'Electronique, LEAME, UMR CNRS 5512, Ecole Centrale de Lyon, F-69131 Ecully Cedex, France*

Received 15 February 1997; accepted 3 March 1997

Abstract

Finite element (FE) analysis, scanning tunneling microscopy (STM), atomic force microscopy (AFM) and transmission electron microcopy (TEM) observations have been used to model stress relaxation in $In_{0.25}Ga_{0.75}As$ layers grown under tension on InP(0 0 1). Ridges or holes are observed at the free surface, depending on growth conditions. TEM observations show that the $In_{0.25}Ga_{0.75}As$ layers are coherently strained and the corresponding strain contrast is simulated using the dynamical electron diffraction contrast theory. The ridge (or hole) strain fields used for the TEM contrast simulations are deduced from FE calculations. These calculations show that elastic stress relaxation mainly occurs at the crest of the ridges or at the edges of the holes and that the underlying substrate is also stressed. To our knowledge, this is the first study describing such various sites of elastic stress relaxation in layers grown under tension.

PACS: 68.55; 73.60.B; 62.40

Keywords: Transmission electron microscopy; Finite element calculations; Elastic stress relaxation

1. Introduction

Semiconductor structures with reduced dimensionality have attracted much interest both for their fundamental properties and for their potential applications in optoelectronics [1, 2]. In an attempt to reach the highest level of confinement (quantum dots), a new method has been recently developed where self-assembling quantum dots are produced directly by molecular beam epitaxy of highly strained InGaAs [3] or InAs [4] on GaAs without processing. It is based on the observation that highly strained heteroepitaxial growth generally results in the formation of islands in the Stranski–Krastanov growth mode. Most of the corresponding studies have been carried out in the case of

* Corresponding author. Fax: + 33 320 43 65 91; e-mail: alain.lefebvre@univ-lille1.fr.

PII S0022-0248(97)00181-4

compressive layers (III–V alloys on GaAs or InP substrates or SiGe on Si). Very little is known of the 2D–3D growth mode transition in the case of layers grown under tension. To our knowledge, only the systems $In_xGa_{1-x}As/InP$ (with $x < 0.53$) [5] and GaAs/InAs [6] are currently being studied. The aim of this paper is to study the surface morphology of $In_{0.25}Ga_{0.75}As$ grown under tension on InP(0 0 1). This morphology is first shown to be characterized by holes and ridges through atomic force microscopy (AFM) or scanning tunneling microscopy (STM). The strain fields associated with these features are then determined by finite element (FE) calculations and used to simulate the transmission electron microscopy (TEM) images of holes and ridges. The comparison between the observed TEM contrasts and computed TEM images provides experimental information on the strain fields associated with holes or ridges and makes it possible to identify the sites of surface elastic strain relaxation.

2. Experimental procedure

Epitaxial layers were grown in a RIBER 2300 molecular beam epitaxy system equipped with in situ reflection high-energy electron diffraction (RHEED) and connected under ultra-high vacuum to a STM analysis chamber [7]. After thermal desorption of the native oxide from an exactly (0 0 1) orientated InP substrate, a 500 nm lattice-matched $In_{0.53}Ga_{0.47}As$ buffer layer was first grown at a substrate temperature of 525°C under As-stabilized conditions. Then, highly mismatched tensilely strained $In_{0.25}Ga_{0.75}As$ layers were grown at 525°C under the following conditions: As-stabilized growth for sample A (V/III beam-equivalent pressure, 85; growth rate, 0.225 μm/h; thickness, 17 monolayers) and As-stabilized growth (V/III beam-equivalent pressure, 23; growth rate, 1.75 μm/h; thickness, 11.5 monolayers) followed by a 10 mn annealing at 525°C under As-reduced conditions after the growth, for sample B. The 2D/3D transition was detected by RHEED at 11 monolayers for sample A, and during the annealing at 525°C for sample B. Ex situ atomic force microscopy images were acquired with various scanning directions on a Digital Instrument microscope operated in tapping mode and using Si tips. In both the cases, characteristic images were acquired at various places on the sample to get a representative picture of the layers. In situ STM images were also taken for sample A because the surface features were not readily analysed by AFM (average dimensions less than 50 nm). They were typically acquired at a tunneling current of 0.2 nA, a sample tunneling voltage in the range $-2.5/+2.5$ V and using electrochemically etched $Pt_{0.8}Ir_{0.2}$ tips.

For the preparation of plan-view TEM thin foils, the samples were mechanically thinned approximately to 30 μm from the substrate side and then ion-milled. TEM studies were performed either with a Philips CM 30 microscope operated at 300 kV or with a Jeol 200 CX microscope operated at 200 kV. The [0 0 1] direction was chosen to be perpendicular to the interface plane and directed towards the epilayer side (epilayer on the top surface of the thin foil, Fig. 1). Two-beam bright-field and dark-field images were taken with $\boldsymbol{g} = 220$ and either digitalized from films with an Agfa Arcus II scanner or directly captured with a slow-scan CCD Gatan camera. The foil thickness and the deviation parameter were locally determined by convergent beam electron diffraction measurements [8]. The simulated TEM images were calculated with a program based on the resolution of the Howie–Whelan equations [9] using the column approximation and the fourth-order Runge–Kutta method, originally employed by Head [10]. Bright and dark field intensities were calculated on two-beams conditions for 200 kV (or 300 kV) and constant foil thickness. The normal and anomalous absorption coefficients were, respectively, taken to be $\xi_g/\xi'_0 = \xi_g/\xi'_g = 0.066$ for 200 kV (or 0.054 for 300 kV) [11, 12].

The displacement field used to carry out the contrast simulations was deduced from finite-element (FE) calculations. These calculations made it possible to vary the shape of the surface defects readily. They were performed using the package ANSYS. These calculations provide nodal displacements that enable the entire stress and strain tensors to be calculated. The sample is modelized as a periodic structure including 3D defects (holes or ridges) quadratically distributed on a 2D flat

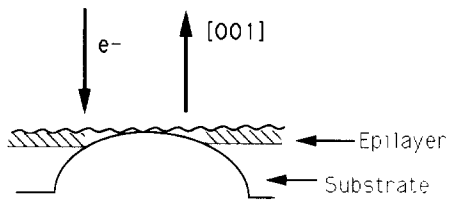

Fig. 1. Schematic view of the $In_{0.25}Ga_{0.75}As/InP$ thinned sample showing the conditions of observation in the electron microscope (the samples were thinned from the substrate side).

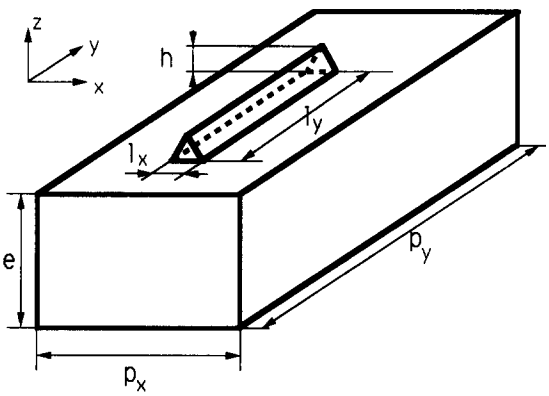

Fig. 2. Illustration of the FE unit cell used in the calculations for a ridge. For holes, h is reversed with regard to $[O_z]$. A truncature can also be introduced at the top of the ridge or at the bottom of the hole.

surface. We can, thus, define a rectangular unit cell built on two perpendicular axes ($O_x \| [1\,1\,0]$) and ($O_y \| [1\,\bar{1}\,0]$) centred on the defect. The calculations are carried out by applying the boundary conditions associated with the periodicity along (O_x) and (O_y): all the nodes of the cell sides are fixed against displacement in the O_x and O_y directions, respectively. The cell dimensions are p_x, p_y, e and the defect dimensions in the cell are l_x, l_y, h (e is the thickness of a whole system including the substrate, the buffer layer and the InGaAs 2D epilayer; h is either the height of the ridge or the depth of the hole; see Fig. 2 in the case of a ridge). The geometry is meshed with 8-node cuboid elements. For the calculations, the lattice mismatch $f = (a_{InP} - a_{In0.25Ga0.75As})/a_{In0.25Ga0.75As}) = 0.020$ between epilayer and substrate is simulated in the framework of thermoelasticity: the strain is introduced by setting the thermal expansion coefficient of the epilayer and the substrate to $-2.0 \times 10^{-2}\,K^{-1}$ and $0\,K^{-1}$, respectively and raising the temperature by 1 K. Young moduli were assumed to be 61.0 GPa (InP) and 76.9 GPa ($In_{0.25}Ga_{0.75}As$) and Poisson ratios were taken equal to 0.360 (InP) and 0.325 ($In_{0.25}Ga_{0.75}As$). Isotropy of the elastic constants was assumed because previous calculations taking into account anisotropic behaviour showed no significant effect [13].

3. Results

Fig. 3a is a STM image of sample A. Well-defined holes elongated in the $[1\,\bar{1}\,0]$ direction and surrounded by misorientated ridges are observed. The average dimensions of these holes are: height, $h = 3.5$ nm; width, $l_x = 30$ nm; length, $l_y = 100$ nm. The angle α between the side facets of the holes and the (0 0 1) plane is about 14°, which corresponds to the (1 0 4) facets, as usually observed on this kind of material [14]. A careful study of the profiles (along x) of holes and ridges has been carried out. The profile displayed in Fig. 3b is characteristic of all these profiles, so that the topography of the surface can be schematized as indicated in Fig. 3c (the lateral average spacing p_x between holes is about two times their average width l_x).

Sample B (Fig. 3d) also exhibits a "hole and ridge" morphology which is much more developed and intricate than for sample A (holes are no longer isolated in this sample). The average dimensions of the ridges are $h = 6$ nm, width $l_x = 50$ nm and length $l_y = 200$ nm. The profile displayed in Fig. 3e is characteristic of all the profiles of holes and ridges studied in this sample, and the topography of the surface can then be schematized as indicated in Fig. 3f (the lateral average spacing p_x between ridges is once again about two times their average width).

Let us now consider the results of TEM observations. Fig. 4a and Fig. 4d show plan-view dark-field images (diffraction vector $\boldsymbol{g} = 220$, deviation parameter $s = -0.7 \times 10^{-2}\,nm^{-1}$) of samples A and B, respectively. Black/white contrasts are lying along the $[1\,\bar{1}\,0]$ direction on a more or less

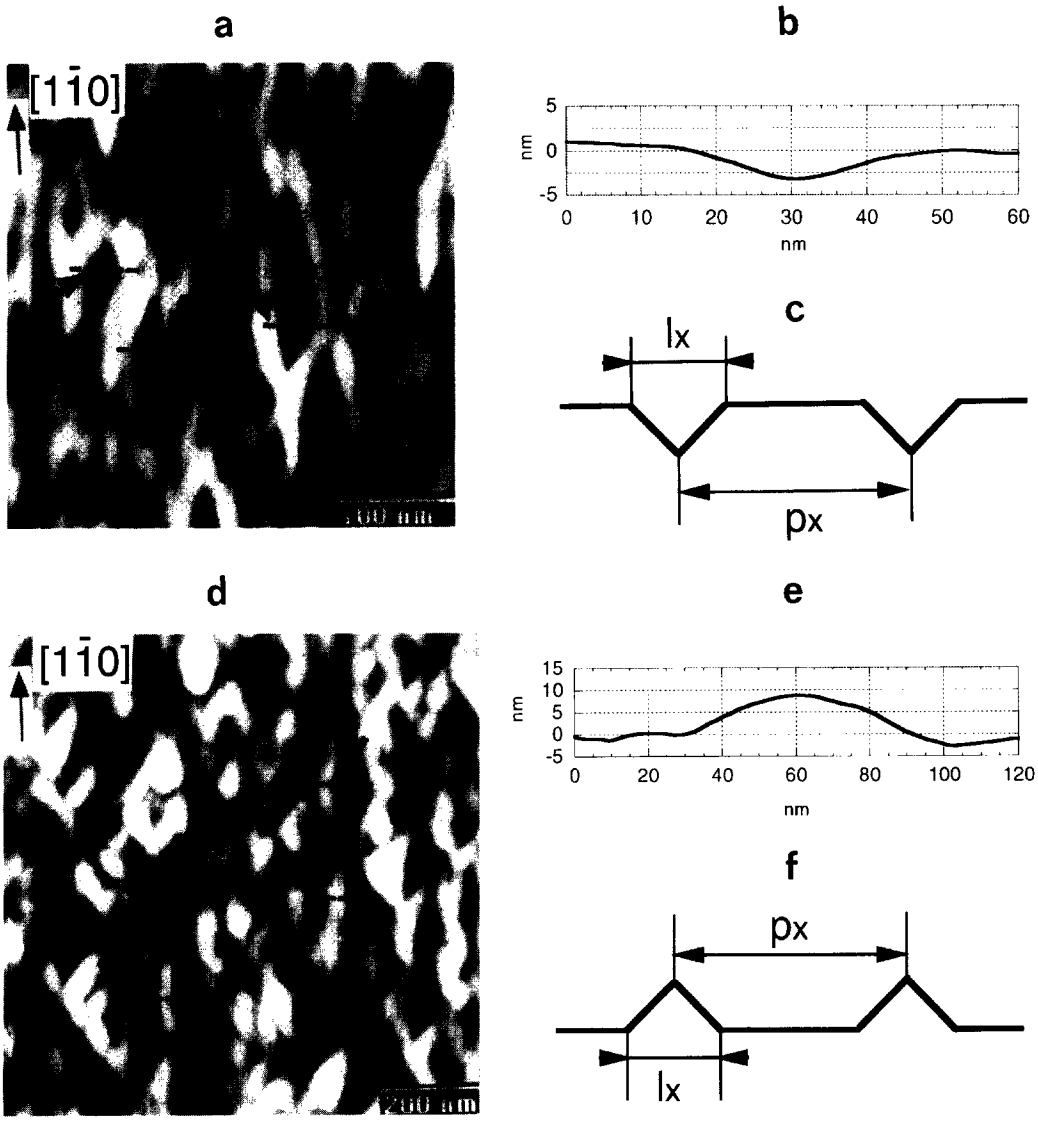

Fig. 3. (a) STM image of sample A. The few arrowed lines indicate where the characteristic profile of Fig. 3b has been obtained. (b) A characteristic profile of the holes and ridges of sample A. (c) Schematic view of the surface topography of sample A. (d) AFM image of sample B. The few arrowed lines indicate where the characteristic profile of Fig. 3e has been obtained. (e) A characteristic profile of the holes and ridges of sample B. (c) Schematic view of the surface topography of sample B.

extended grey background. These contrasts are caused by inhomogenous lattice strain associated with 3D surface defects [13, 15–17]. For each black/white contrast, we can define a vector $\boldsymbol{L}$ which points from the centre of the white part of the contrast to the centre of the black part (see Fig. 4b and Fig. 4e), which leads us to the conclusion that, for the diffraction vector $\boldsymbol{g} = 220$, $\boldsymbol{L}$ is always parallel to $\boldsymbol{g}$ for sample A and always antiparallel to $\boldsymbol{g}$ for sample B (inversion of contrast from A to B). It should be noted that this important feature was observed with the conditions of Fig. 1 (epilayer on the top surface of the thin foil) and that this characteristic is still valid with the epilayer on

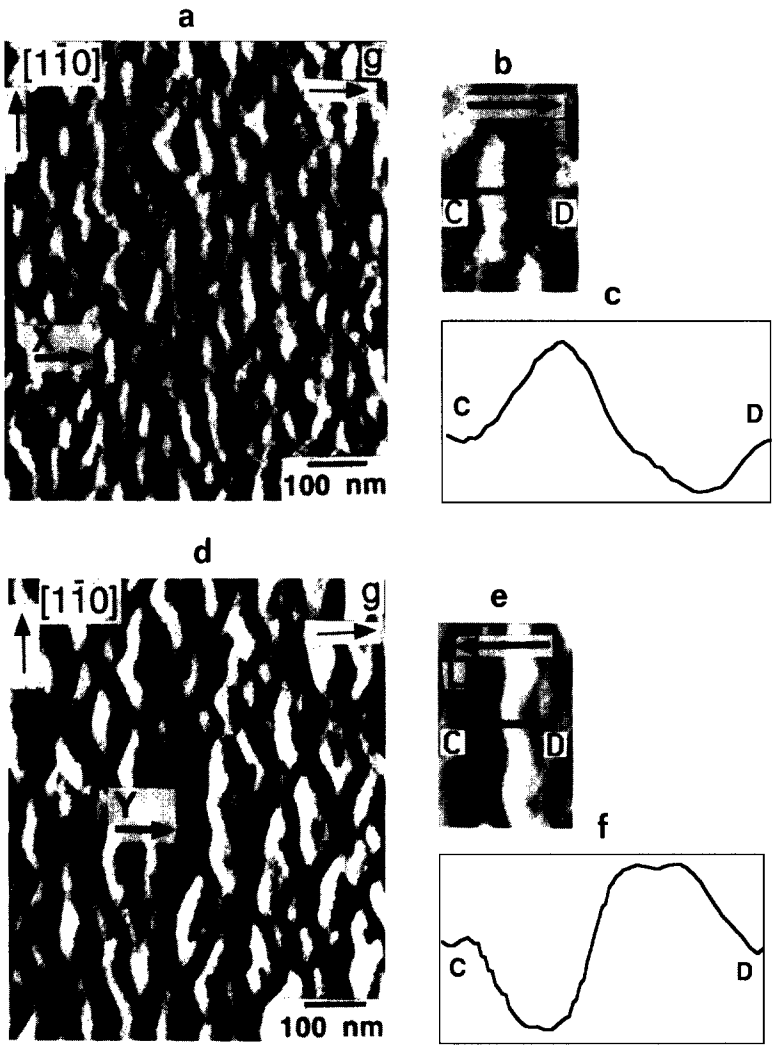

Fig. 4. (a) Dark-field TEM micrograph of sample A; $\boldsymbol{g} = 220$, $s = -0.7 \times 10^{-2}\,\mathrm{nm}^{-1}$. (b) Enlargement of the area labelled X in (a). (c) Intensity profile along the line CD as defined in (b). (d) Dark-field TEM micrograph of sample B; $\boldsymbol{g} = 220$, $s = -0.7 \times 10^{-2}\,\mathrm{nm}^{-1}$. (e) Enlargement of the area labelled Y in (d). (f) Intensity profile along the line CD as defined in (e).

the bottom surface of the thin foil (this is no longer valid in the case of bright fields and this point will be further analysed in the discussion). It should also be noticed that a slight modulation is observed inside the white lobes associated with sample B, whereas no modulation is observed in the white/black lobes associated with sample A (see the profiles of Fig. 4c and Fig. 4f).

In order to explain the observed contrast inversion between A and B with $\boldsymbol{g} = 220$, TEM intensity calculations have been performed using FE displacement fields associated with 3D faceted holes and ridges elongated in the [1 $\bar{1}$ 0] direction. These FE calculations have been carried out on 3D models with the following parameters as deduced from the AFM and STM observations: $h/l_x = 0.12$, $p_x/l_x = 2$, $l_x/l_y = 0.33$, $p_x/p_y = 0.66$ and $\alpha = 14°$. The substrate thickness was chosen to be 100 nm and it was checked that the FE results were not affected as long as the thickness was not lower than 50 nm.

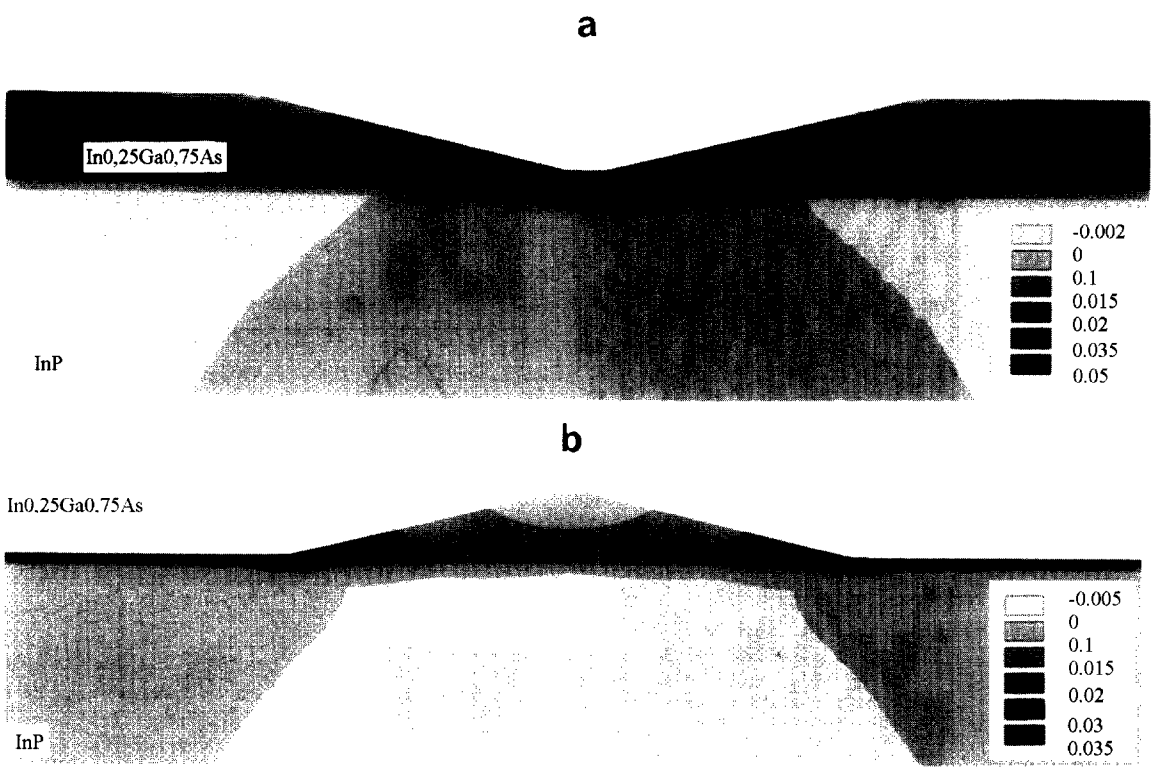

Fig. 5. Strain field component ε_{xx} (with $y = 0$) as calculated by the FE method. (a) Hole in the $In_{0.25}Ga_{0.75}As$ layer. (b) Ridge in the $In_{0.25}Ga_{0.75}As$ layer.

Only the component $u_x([O_x] \| [1\ 1\ 0])$ of the displacement $\boldsymbol{u}$, parallel to $\boldsymbol{g}$, is needed for TEM calculations with the column approximation. However, results on the strain component ε_{xx} (with $y = 0$) are displayed in Fig. 5, owing to their clearer physical meaning. In both cases (hole or ridge), a significant stress relaxation occurs in the thicker regions (top of the ridge and edges of the hole) and stress concentration in the thinner regions (edges of the ridge and bottom of the hole). A significant tensile strain is also observed in the substrate under the thinner regions and a compressive strain under the thicker regions of the epilayer (the occurrence of such a strain had already been suggested or demonstrated in the case of epilayers strained under compression [13, 17–20]). Nevertheless, strain in the underlying substrate remains weak when compared to that existing in the epilayer.

Fig. 6a and Fig. 6b show the results of the TEM contrast calculations (intensity profiles along O_x), respectively, on holes and ridges, with $\boldsymbol{g} = 220$, $s = -0.7 \times 10^{-2}\ \mathrm{nm}^{-1}$ and sample thickness $t = 270$ nm. As might have been expected, they are made up of black and white lobes with an inversion of contrast between Fig. 6a and Fig. 6b. The experimental profiles of Fig. 4c and Fig. 4f are characteristic of all the profiles that have been obtained from experimental digital images such as those of Fig. 4a and Fig. 4d. The comparison of calculated contrasts (in Fig. 6) and experimental contrasts (in Fig. 4c and Fig. 4f) shows that the contrast obtained on sample A must be associated with a hole (compare profiles in Fig. 6a and Fig. 4c) whereas the contrast obtained on sample B must be associated with a ridge (compare profiles in Fig. 6b and Fig. 4f). Those simulated contrasts also exhibit the white lobe's slight modulation for the ridge and no modulation for the hole, which is consistent with experimental observations.

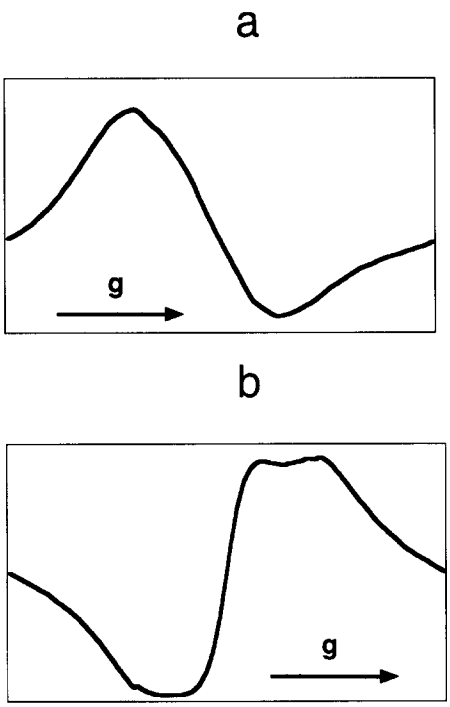

Fig. 6. Computed TEM image contrast profiles ($\boldsymbol{g} = 220$, $s = -0.7 \times 10^{-2}$ nm^{-1}, $t = 270$ nm) in the case of a hole (a) or in the case of a ridge (b).

4. Discussion and conclusion

Our previous studies of InAs quantum dots on a GaAs substrate had emphasized the validity of the FE approach for calculating 3D defect strain fields and for simulating the TEM contrasts of such defects [13]. In the present paper, using this method made it possible to localize the various sites of stress relaxation occurring at the surface of $In_{0.25}Ga_{0.75}As$ layers grown on InP under tension: for sample A, stress relaxation occurs at the edge of holes whereas it occurs at the top of ridges for sample B. More generally, it should be noted that the identification of these various sites (ridges or holes) can be readily made with TEM bright-field or dark-field observations by comparing the sense of vectors $\boldsymbol{g}$ and $\boldsymbol{L}$ and using the rules described in Figs. 7 and 8. These rules were established for epilayers either under tension or under compression and situated either on the bottom surface of the thin foil, or on the top face of the thin foil. They were deduced from the simulations of TEM contrasts and it was checked that they were consistent with the general results obtained by Ball [21] and Katerbau [22].

The TEM contrasts of islands are known to be very sensitive to the shape of these defects, as emphasized in other references [13, 16, 17]. In particular, for islands under compression (InAs/GaAs), the modulation of the black and white lobes of the TEM images is all the higher as the islands are truncated. We have checked that it was still true in the case of epilayers under tension, for holes as well as for ridges. The absence of modulation in the hole TEM images and the slight modulation of the ridge TEM images are consistent with V-shaped holes or ridges, which fully confirms the results of STM and AFM observations.

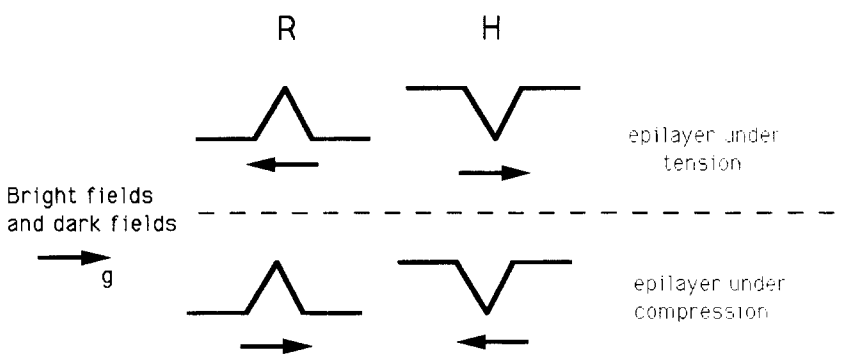

Fig. 7. Sense of vector L for epilayers lying on the top surface of the thin foil. R = ridge. H = hole. $\boldsymbol{g} = 220$, $s = 0$.

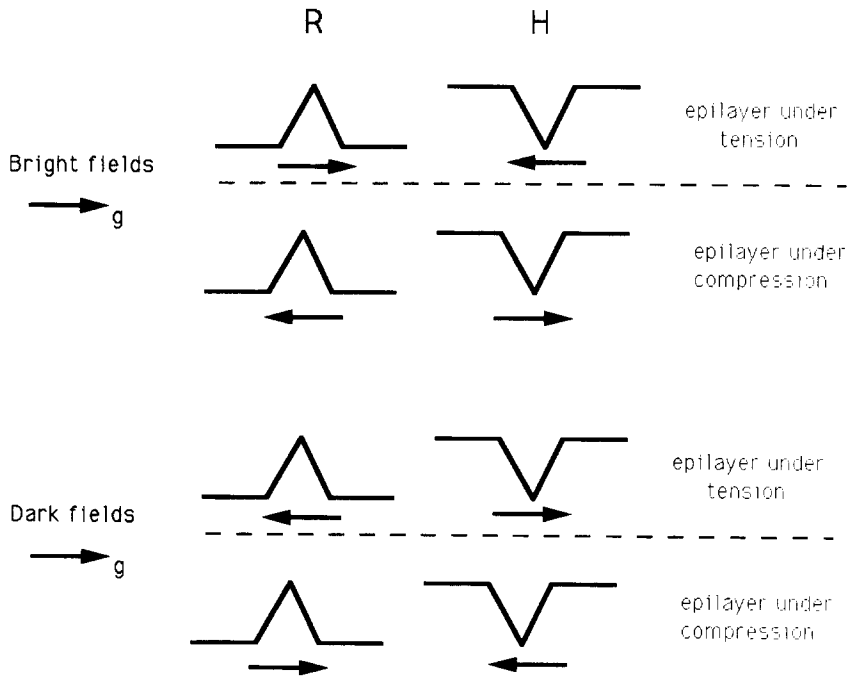

Fig. 8. Sense of vector L for epilayers lying on the bottom surface of the thin foil. R = ridge. H = hole. $\boldsymbol{g} = 220$, $s = 0$.

References

[1] M. Asada, Y. Miyamoto, Y. Svetmasu, Jpn. J. Appl. Phys. 24 (1985) L95.
[2] C. Weisbuch, G. Vinter, in: Quantum Semiconductor Structures, Academic Press, Boston, MA, 1991.
[3] D. Leonard, M. Krishnamurty, C.M. Reaves, S.P. Denbaars, P.M. Petroff, Appl. Phys. Lett. 63 (1993) 3203.
[4] J.M. Moison, F. Houzay, F. Barthe, L. Leprince, E. André, O. Vatel, Appl. Phys. Lett. 64 (1994) 196.
[5] M. Gendry, V. Drouot, C. Santinelli, G. Hollinger, J. Appl. Phys. 60 (1992) 2249.
[6] G. Attolini, E. Chimenti, P. Franzosi, S. Gennari, C. Pelosi, P.P. Lottici, Appl. Phys. Lett. 69 (1996) 957.
[7] L. Porte, P. Krapf, Y. Robach, M. Phaner, M. Gendry, G. Hollinger, Surf. Sci. 352 (1996) 60.
[8] P.M. Kelly, A. Jostsons, R.G. Blake, J.G. Napier, Phys. Status Solidi (a) 31 (1975) 771.
[9] P.B. Hirsch, A. Howie, R.B. Nicholson, R.B. Pashley, M.J. Whelan, in: Electron Microscopy of Thin Crystals, ch. 10, Krieger, New York, 1977.
[10] A.K. Head, Aust. J. Phys. 20 (1967) 557.
[11] A.K. Head, P. Humble, L.M. Clarebrough, A.J. Morton, C.T. Forwood, in: Computed Electron Micrographs and Defect Identification, North-Holland, Amsterdam, 1973.
[12] D.M. Bird, Q.A. King, Proc. 47th Annual Meeting of the Electron Microscopy Society of America, San Francisco Press, San Francisco, 1989, p. 486.
[13] T. Benabbas, P. François, Y. Androussi, A. Lefebvre, J. Appl. Phys. 80 (1996) 2763.
[14] A. Ponchet, A. Le Corre, A. Godefoy, S. Salaün, A. Poudoulec, J. Crystal Growth 153 (1995) 71.
[15] J.Y. Yao, T.G. Anderson, G.L. Dunlop, J. Appl. Phys. 69 (1991) 2224.
[16] Y. Androussi, P. François, A. Lefebvre, C. Priester, I. Lefebvre, G. Allan, M. Lannoo, J.M. Moison, N. Lebouché, F. Barthe, in: B.G. Demczyck, E. Garfunkel, B.M. Clemens, E.D. Williams, J.J. Cuomo (Eds.), Evolution of Thin film and Surface Structure and Morphology, Mater. Res. Soc. Proc., vol. 355, 1994, pp. 569–574.
[17] Y. Androussi, A. Lefebvre, B. Courboulès, N. Grandjean, J. Massies, T. Bouhacina, J.P. Aimé, Appl. Phys. Lett. 65 (1994) 1162.
[18] D.J. Eaglesham, M. Cerullo, Phys. Rev. Lett. 64 (1990) 1943.
[19] S. Guha, A. Madhukar, K.C. Rajkumar, Appl. Phys. Lett. 57 (1990) 2110.
[20] S. Christiansen, M. Albrecht, H.P. Strunk, P.O. Hansson, E. Bauser, Appl. Phys. Lett. 66 (1995) 574.
[21] C.J. Ball, Phil. Mag. 9 (1964) 541.
[22] K.H. Katerbau, Phys. Status Solidi (a) 59 (1980) 211.